

3D high viscosity jetting of functional materials

Javier Ledesma-Fernandez, Christopher Tuck, Richard Hague; Additive Manufacturing and 3D Printing Research Group (3DPRG), University of Nottingham; Nottingham, United Kingdom

Abstract

Inkjet printing is one of the most suitable technologies to produce multi-material and multi-layered printed electronics due to its scalability, the wide range of substrates that it can accept and the possibility of mixing and combining numerous fluids in a single process. However, restrictions in material properties such as viscosity, typically below 25 mPa·s, limit the molecular weight of usable polymers and the solid content of inks. In some cases, this leads to volumetric shrinkage, longer post-process treatments and poor performance. Therefore, a high viscosity approach would widen the material catalogue for printed electronics without compromising the advantages of inkjet.

In this work, drop-on-demand micro-dispensing valves that combine mechanic and pneumatic actuation were used to create 2D patterns and 3D structures of a conductive and non-Newtonian carbon paint. The combination of this functional material with a non-conductive photo-curable resin allowed the creation of more complex 3D geometries using the layer-by-layer approach typical from Additive Manufacturing. Printing parameters such as pneumatic pressure, valve closing speed, resolution and drying time are studied and optimised to produce multi-layered tracks, self-standing pillars and a functional demonstrator featuring a printed capacitive switch and an embedded commercial LED.

Introduction

The rise and consolidation of digital fabrication have made possible the manufacture of highly customised and complex products in almost every industry. This not only allows the creation of devices that were impossible just a few decades ago but also facilitates the production of small runs of products at a reasonable cost, which reduce the designing-prototyping cycles and boosts innovation. This next step in manufacturing has not been unnoticed by the electronics industry, whose fast pace require constant improvement, but this sector also introduces several challenges that traditional techniques cannot easily overcome. Particularly, even though well-established techniques such as screen printing [1] and reel-to-reel flexographic printing [2] have been successfully used to produce electronic tracks and devices on industrial scales, they are not ideal for the creation of complex 3-dimensional (3D) structures. This limitation comes from the requirement of different 2D patterns of the layer-by-layer approach, which in the aforementioned examples would imply as many screen or plate designs as layers on the object, increasing the total cost and time of the process.

A more suitable technology to tackle the production of multi-material 3D parts could be inkjet printing, which is capable of depositing fluids in a drop-on-demand non-contact fashion on a variety of substrates, limiting also the amount of wasted material. Additionally, it offers the possibility of mixing and placing different inks alongside each other, raising even more the complexity of the achievable parts without a

necessary increase in the cost. In fact, inkjet printing has already demonstrated its fitness to the electronic industry with the printing of devices such as functional transistors [3], strain sensors on fabric [4] or low-cost Radio-frequency Identification (RFID) tags [5]. However, inkjet imposes great restrictions on the properties of the inks that need to be carefully formulated to avoid nozzle clogging, exhibit long stability during storage and behave according to predictive models during the printing process. A major consequence of these restrictions is that the viscosity of the inks needs to remain typically under 25 mPa·s, which limits the molecular weight of the used polymers and the solid content of particulate inks. This not only narrows the material catalogue but also forces the addition of rheological modifiers such as solvents and surfactants that alter the properties of the deposited tracks [6]. It is especially relevant in the case of conductive materials, where the organic elements added to improve the processability of the ink need to be removed during a post-processing step to allow the percolation or sintering of the conductive particles dispersed in the ink.

Therefore, a high viscosity approach would allow the deposition of inks or pastes with higher solid content, which translates into reduced volumetric shrinkage, increased mechanical properties and improved conductivity. This has been explored by different methods such as aerosol jet [7], where the material is atomized in a pressurized chamber prior to deposition; acoustic inkjet, where an ultrasonic perturbation is focused on the fluid free surface to induce the creation of droplets without the need of a nozzle [8]; and ultrasonic droplet generation, where the nozzle plate is specifically designed to focus the acoustic waves generated by a piezoelectric actuator and produce the ejection of droplets [9]. Alternatively, jetting valves that combine mechanical actuation and pneumatic pressure to overcome the surface tension and elastic components of the viscosity have also been used to create 2D-patterns in a continuous inkjet approach [10] [11].

In the present work high viscosity jetting is explored to deposit discrete drops of carbon paste and a photo-reactive resin to create 2- and 3-dimensional structures. However, before producing these structures, an overview on the optimization of the main printing parameters will be given.

Materials and methods

Materials

A water-based carbon paint (Electric Paint, Bare Conductive) was chosen as a conductive and soluble support material and was used as received and within its recommended shelf life. The bottle was sealed and kept in an extra container, also sealed, to avoid solvent evaporation. Its resistivity was measured in earlier work as $1.09 \pm 0.03 \cdot 10^{-2} \Omega \cdot m$ [11].

A transparent photo-curable resin (Clear, Formlabs) with a curing wavelength of 405 nm was selected as a structural material, which was also used without any modification. This fluid was kept in a sealed amber bottle capable of blocking UV-radiation to prevent partial curing before printing.

The embedded LED used in the demonstrator was a green PICOLED (P12 Series, ROHM) of 1.0 x 0.6 x 0.2 mm and was placed manually with a pair of tweezers between printing cycles. Its position was checked with the mounted camera of the printing stage and it was powered and controlled using an open source micro-controller (Arduino UNO, Arduino).

High viscosity printing system

The set-up consists of two identical micro-dispensing valves (PICO xMOD, Nordson EFD) mounted on a computer-controlled 3-dimensional stage with an overall accuracy of 5 µm. The system is also equipped with a monochrome digital camera (Manta, Allied Vision Technologies GmbH) to monitor the printed patterns and select the printing origin. A UV-lamp (FireFly 25x10, Phoseon Technology) was installed to enable photo-curing of materials during the process. The software is based on a combination of C# and XML and is in charge of printing parameters such as printing speed, resolution (DPI) and curing speed. This code also communicates with the digital controller that provides the printing signal to the valves.

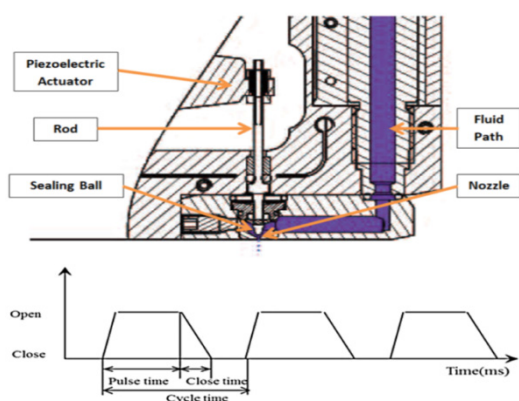


Figure 1. (Top) Schematic illustration of the micro-dispensing valve with a description of its most relevant parts. Modified from valve user manual [12]. (Bottom) Description of the relevant parts of the driving pulse and its effect on the nozzle state.

The working principle of the jetting valve is based on the combination of mechanic and pneumatic actuation. Specifically, the fluid is pressurized (up to 0.6 MPa) and injected on the jetting chamber along a fluid path that can be heated up to 100° C. There, a piezo-electrically driven plunger ended with a ceramic sealing ball is oscillated according to the printing signal (up to 500 Hz), opening and closing the nozzle as a consequence. These driving pulses are mainly described by its pulse time (t_p) and cycle time (t_c), which are set on the digital controller, and the opening and closing speed, which is not under user control but can be selected from a limited amount of pre-sets. This system allows the ejection of materials in the range of 50 – 200.000 mPa·s [12] through a nozzle of 50 µm in diameter. A schematic illustration of this system is shown in Figure 1 along with a description of the printing pulses.

Viscosity characterization

The viscosity of the materials was measured with a combination of two different rheometers to map different ranges of shear rate. The low shear region is here referred to as the range of shear rates between 1 s⁻¹ and 1000 s⁻¹ and was measured with a rotational rheometer (Kinexus Pro, Malvern Instruments Ltd.) with a cone-plate configuration. However, for

the carbon paint, the maximum shear rate achievable before the sample was driven outside the plates of the instrument was 100 s⁻¹. The measurements were performed leaving sufficient time for the fluids to rest between the plates of the rheometer to allow their micro-structure to reform after the sample loading process while the evaporation of the solvent (relevant for the carbon sample) was prevented using a solvent trap saturated with water vapour. Each curve was measured 3 times and averaged, the uncertainty in all cases was below 5%. The temperature was kept at 25° C, which is the intended temperature during printing.

The high shear region was measured with a microfluidic rheometer (hts-VROC, RheoSense) equipped with a channel of 100 µm width containing 3 embedded Micro Electro Mechanical System (MEMS) pressure sensors along its length. In this case the applied pressure of the system is fixed but the flow rate and achievable shear rate is determined by the combination of the depth of the micro-channel, the syringe used (1 ml in this case) and the viscosity of each sample. Consequently, the carbon paste was tested between 80 and 2500 s⁻¹, while the photo-reactive resin was measured in the range of 1000 and 9000 s⁻¹. In order to obtain the true shear rate and viscosity, the instrument automatically applies the Weissenberg-Rabinowitsch-Mooney (WRM) correction [13]. In both cases the experiment was performed 3 times at a constant temperature of 25 °C and the data averaged. The uncertainty in this case was lower than 3%.

Jettability and deposition study

The footprints of deposited drops on polycarbonate (PC) films resulting from different settings of pressure (0.1 – 0.5 MPa) and valve closing time (120 – 400 µs) were studied with an optical microscope (Eclipse LV100 ND, Nikon) in reflection configuration. Its associated software (NIS-Elements) was used to automatically obtain the perimeter (P) and area (A) of the droplets, which are used to calculate their equivalent diameter and circularity with the intention of assessing their repeatability. Precisely, the equivalent diameter (d_{eq}) is the diameter that each drop would have according to their area if their shape was perfectly circular, as shown in (1). The circularity (f_{circ}) was calculated according to its definition (2) and would be 1 for the case of an ideal circumference:

$$d_{eq} = 2 \sqrt{\frac{A}{\pi}} \quad (1)$$

$$f_{circ} = \frac{4\pi A}{p^2} \quad (2)$$

Tests at different resolutions (measured in drops per inch, DPI) and in situ monitoring of the printed layers was performed with the monochrome digital camera mounted on the carrier of the printing stage.

Post-printing processes investigation

UV-curable materials were post-processed with a UV-lamp of 2 W/cm² peak irradiance and 380 – 420 nm output (FireFly 25x10, Phoseon Technology) at 4.0 mm ± 0.1 mm of the printing platform. The sample is moved under the lamp at a constant speed referred to as the curing speed. Materials requiring evaporation of solvent between layers were left to dry at monitored temperature and constant humidity. To further study the linearity of the height of the samples with successive layers, multi-layered tracks were printed, allowed to rest during 24 h and later characterised with a surface profilometer (SurfTest SV-3100, Mitutoyo).

Results and discussion

Viscosity characterization

The viscosity of the carbon paste and the photo-curable resin was studied at different shear rates at 25°C, as can be seen in Figure 2. The lower shear rates were measured with a rotary rheometer with a cone and plate configuration while the high shear rates were measured with a microfluidic rheometer, obtaining with both systems compatible results. The carbon paint displays a typical “shear thinning” behaviour, since its viscosity decreases with the increment of shear rate, which is common for composites with significant solid loading [14]. Specifically, it is observed to go from $55 \pm 3 \text{ Pa}\cdot\text{s}$ at 0.1 s^{-1} to $3.68 \pm 0.06 \text{ Pa}\cdot\text{s}$ at 1095 s^{-1} . This is particularly helpful since in storage conditions the material presents a very high viscosity, which helps to maintain the micro-flakes of carbon in suspension and preserves the stability of the paint. On the other hand, when the material is carried along the pipes of the system and ultimately jetted at high shear rates, the viscosity is lower, improving the processability of the material [15]. Alternatively, the viscosity of the photo-reactive resin does not change significantly in the range of shear rates investigated and the material can be categorized as Newtonian for the purposes of this work, the average value for the shear viscosity is $818 \pm 6 \text{ mPa}\cdot\text{s}$. In Figure 3 the relation between the shear stress and the shear rate is plotted for both materials, which confirms the Newtonian behaviour of the photo-polymer and reveals a non-negligible yield stress for the carbon paint typical from Bingham plastics [16].

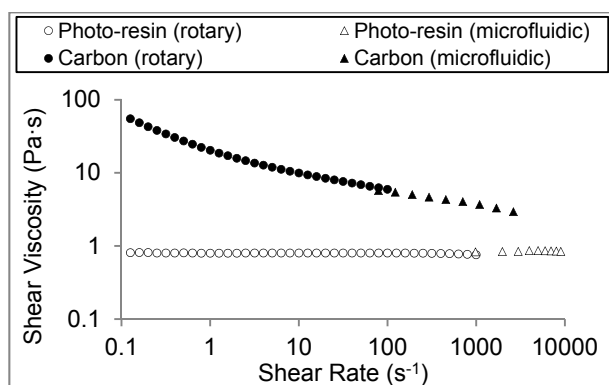


Figure 2. Flow curve of carbon paint and photo-curable polymer at 25°C measured by a combination of a rotary and a microfluidic rheometer.

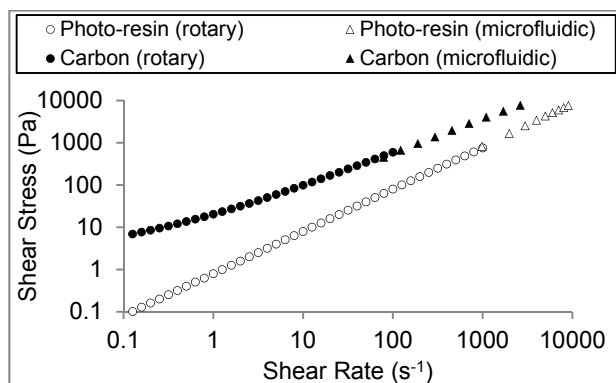


Figure 3. Shear stress dependency on the shear rate for carbon paint and photo-curable polymer at 25°C measured by a combination of a rotary and a microfluidic rheometer.

Jettability and deposition study

Drop formation and deposition

In order to choose the most appropriate values for the pneumatic pressure and the mechanical closing speed of the valve, different combinations of such variables were tested keeping constant other printing parameters such as the temperature (25° C), frequency (95 Hz), pulse time (2 ms) and the distance between the nozzle and the substrate (0.8 mm). These values were chosen based on previous experience with the same set-up [11]. Particularly relevant in the previous study was the observation via high speed video (18000 frames per second) that for these materials the ejection only happens during the closing of the valve, since the applied pressure is not enough on its own to initiate the flow through the nozzle. This explains why, as long as the pulse time is enough to raise the plunger completely, its length is not relevant. Additionally, from the mentioned videos it was also observed that a relevant factor for drop ejection and repeatability is the amount of material left behind on the outside of the nozzle plate after each stream of material is emitted. Specifically, if there is a significant volume of fluid on the outside of the nozzle the next drop would encounter a higher resistance than the previous one but would have the same kinetic energy, which leads to a higher material residue with each iteration until the ejection is eventually prevented. However, even though many conclusions can be extracted from the observations of high speed videos of the ejection with different printing parameters it is still a method that will require an external set-up, which is not ideal in terms of the speed of the optimization cycle of each material. Therefore, an approach closer to machine vision is used in this case, analysing with a microscope and a digital camera the samples produced by the main printing set-up, as can be seen in Table 1. Later the area and perimeter of each drop was automatically detected and used to plot the equivalent diameter and the circularity for each material and configuration, as is shown in Figure 5 and Figure 4.

Table 1. Droplets obtained with different combinations of valve closing time and pneumatic pressure

Closing time	Carbon Paint			Photo-curable resin		
	0.1 MPa	0.3 MPa	0.5 MPa	0.1 MPa	0.3 MPa	0.5 MPa
400 μs				No droplets generated		
200 μs						
120 μs						

In the case of the carbon paint, it was observed that there is not a clear trend relating the pneumatic pressure with the size and shape of the drops. This is in agreement with the previously observed ejection of the material only during the closing time of the valve and limits the role of the pressure to filling the nozzle chamber to avoid material stagnation. Nonetheless, there is a greater variation in the circularity of the drops with pressure for the slowest closing profile (400 μs), but this seems more likely to be related with the closing time, since these drops are slower and therefore their tail breaks in a more

uncontrollable way, as can be observed in Table 1. On the contrary, the fastest profile (120 μ s) produces bigger drops with good repeatability, which is due to the fastest speed of the drops and their spreading on the substrate governed mainly by kinetic effects. Still, this configuration showed signs of splashing; indicating that the ejection speed was excessive. The profile with a closing time of 200 μ s provides small drops (diameter of 391 ± 2 μ m at 0.1 MPa) and good repeatability across different pressures and was consequently selected for the rest of the work.

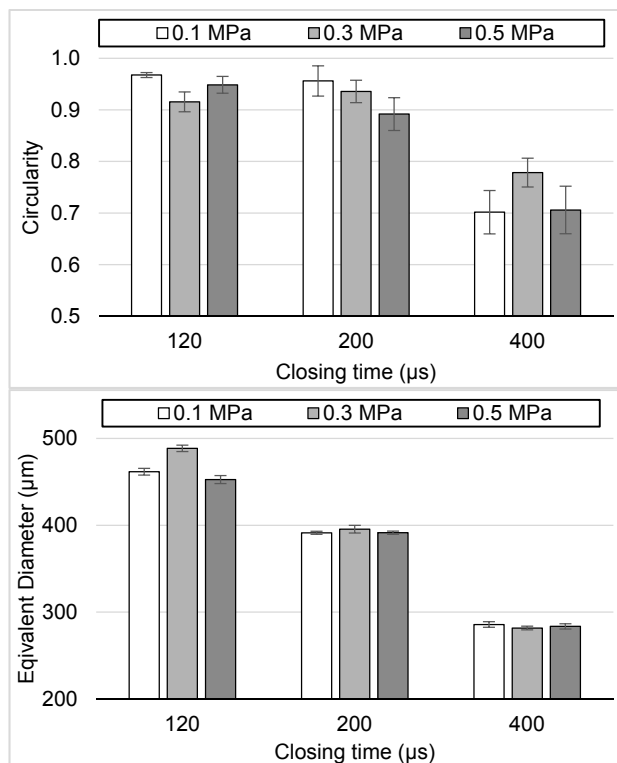


Figure 4. Circularity (top) and equivalent diameter (bottom) calculated from droplets of carbon paint at different pneumatic pressure and valve closing speed, as shown in Table 1.

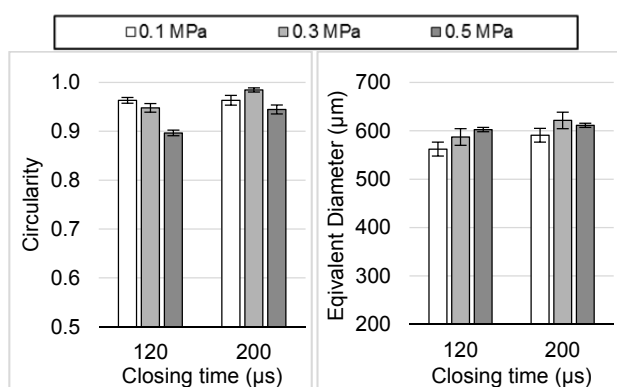


Figure 5. Circularity (left) and equivalent diameter (right) calculated from droplets of photo-polymer at different pneumatic pressure and valve closing speed, as shown in Table 1.

Regarding the photo-reactive resin, the first thing that stands out is the lack of drops with the slowest profile (400 μ s), which indicates that the kinetic energy administrated by the valve is insufficient to overcome other effects like the surface tension and the elastic components of the viscosity.

Still, this was only tested within the pressure range achievable by the set-up and it is expected that a higher pressure would eventually induce ejection on its own. Additionally, high circularity and smoothness are observed for both successful profiles, which is attributed to its wetting behaviour, ruled by its low surface tension 34.9 ± 0.2 mN·m⁻¹ [11] and the lack of a significant yield stress, as shown in Figure 3. However, the profile with a closing time of 200 μ s shows more repeatable results across different pneumatic settings, and was therefore selected for the rest of this report together with a pressure of 0.1 MPa, yielding drops of 591 ± 2 μ m in diameter.

Once the drop formation and deposition were satisfactory, different square patterns were printed with resolutions between 50 DPI and 250 DPI, as shown in previous work [11]. The optimum resolution is accepted as the one that yields patterns with connected drops without leaving holes but also presents edges as straight as possible without instabilities due to excessive fluid per unit area. In the case of the carbon paint the chosen resolution was 100 DPI, which corresponds to an overlap of 35%, while a DPI of 60 (28% overlap) was selected for the photo-resin, as it is shown in Figure 6.

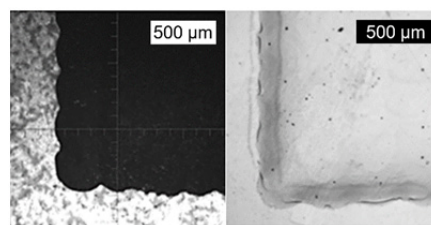


Figure 6. The printing resolution for each material is determined by looking at the corner of a printed square pattern. This tests resulted in a resolution of 100 DPI for the carbon paste (left) and 60 DPI for the UV-curable polymer (right).

Post-treatment and multi-layer tests

The layer-by-layer approach to the fabrication of 3-dimensional structures requires that each layer of material is deposited and treated before placing the next one, in order to avoid curved substrates and fluid coalescence between layers. This depends strongly on the post-treatment method chosen for each material. Specifically, the carbon paste was allowed to evaporate at 25°C during a certain period of time (0, 30 and 300 s) before printing the next layer, whereas the photo-curable resin was treated with a moving UV-lamp at constant height (4 mm) but different translational speeds (6 mm/s and 150 mm/s) to modify the photonic energy delivered to the material. Following the described methodologies for printing and post-treatment, samples with 8 tracks of an increasing number of layers from 1 to 8 were produced for the different settings, as can be seen in Figure 7. The results for the transparent resin are indistinguishable by mere observation and require further analysis but this is not the case for the carbon, where it is clear that both 0 and 30 seconds were too short to allow total evaporation and linear growth in the Z-direction. This is particularly obvious in the 7th and 8th tracks in both samples, where a bulging effect due to the excess of fluid can be observed. This, however, does not seem to happen to the sample allowed to dry 5 minutes between layers, so this time was accepted as a valid drying process. These conclusions however cannot be generalised since the drying time is strongly related with the area exposed to air, which in turn would depend on the particular pattern. Nonetheless, this test provides a good estimation for processing purposes.

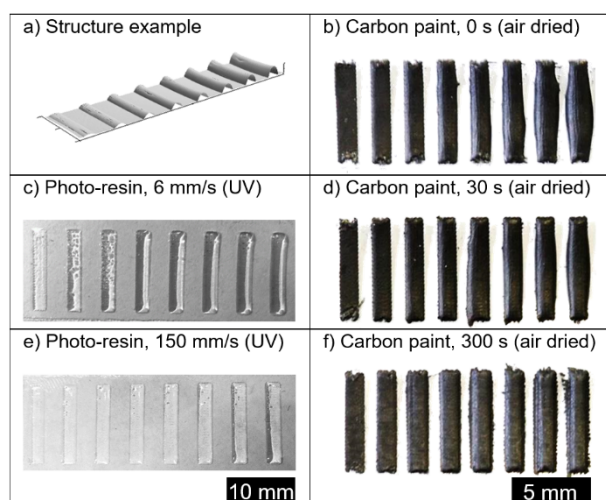


Figure 7. Multi-step structures with growing number of layers (a) were produced with different kinds of post-treatments after each layer. The carbon samples (b,d,f) were allowed to dry at 25°C while the photo-polymer (c,e) was cured by a UV-lamp at different speeds.

To further study the linearity of the height of the samples with successive layers, they were allowed to rest during 24 h and later characterised with a surface profilometer to obtain the height values per layer shown in Figure 8. Later, a linear regression was applied to the 3 sets of data to assess said linearity, as can be seen in Table 2. In the three cases the linear trend is maintained until the 8th step, indicating that consecutive layers are not exchanging material as it was observed for the carbon with short drying times. However, for the photo-resin the slower treatment seems to lead to a lower growth in Z-direction despite delivering more energy to the sample. A possible explanation for this is the fast spreading of the fluid, which is pinned in place earlier with the 150 mm/s curing speed than with 6 mm/s, leading to an overall higher layer thickness. Therefore, 150 mm/s is accepted as the curing speed for this material not only for resulting in slightly thicker deposited layers but also because of its positive impact on the total speed of the process.

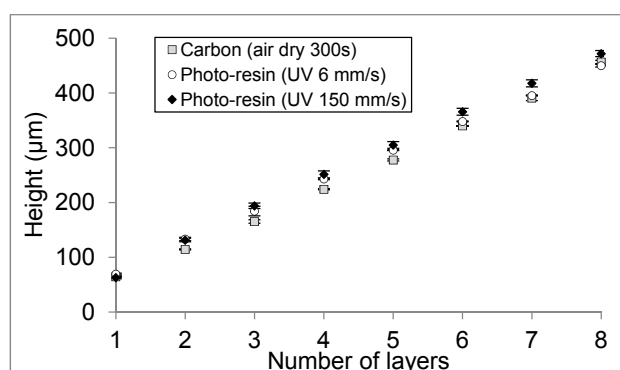


Figure 8. Height evolution of three samples produced with different post-treatments after each layer.

Table 2. Results of a linear regression ($y = m \cdot x + b$) for various post-treatment processes applied to both materials

	Carbon (air dry, 300 s)	Photo-resin (UV, 6 mm/s)	Photo-resin (UV, 150 mm/s)
m	$56 \pm 1 \mu\text{m}$	$58 \pm 1 \mu\text{m}$	$54 \pm 1 \mu\text{m}$
b	$2 \pm 4 \mu\text{m}$	$14 \pm 5 \mu\text{m}$	$23 \pm 4 \mu\text{m}$
r ²	0.9989	0.9986	0.9989

3-dimensional structures

Self-standing pillars

In order to initially explore the 3-dimensional capabilities of this approach, arrays of drops were jetted and post-treated several times in order to create straight pillars, as can be seen in Figure 9. Apart from opening the possibility of interconnections in 3-dimensions, these pillars also reveal a few interesting features of the process itself. For instance, their width is thinner than the diameter of individual drops for both materials. This is explained by the fact that the first drop lands on the substrate (polycarbonate film) but the rest land on top of solid convex material, therefore affecting its wettability. Also, some of the material flows on the sides, increasing the width of the base but maintaining a fairly constant the width of the pillar, which is particularly evident with the photo-resin structures. On the other hand, the UV-curable polymer seems to bond to itself without forming interlayers, which is the reason why these pillars display an almost undisturbed transparency. In the case of the carbon, however, horizontal lines delimit the interface between layers.

Once pillars perpendicular to the substrate were proven, a similar process was followed to print tilted structures, with the only modification of shifting the patterns after every layer. This approach did not succeed for the photo-resin, whose smooth surface and fast spreading lead to elongated puddles instead of pillars. Nevertheless, pillars with 12° and 21° of inclination were successfully printed with the carbon paint (Figure 9), using a shift of 1.0 and 1.5 % respective to the drop spacing at 30 DPI (847µm). It can be observed that 21° seems to be beyond the critical angle, since there is a noticeable amount of material at the base of the pillars. However, in this case it seems unlikely that it has so much to do with the flow of material along the pillar itself but with the landing position and speed of the consecutive drops. Specifically, if the shift is too big each drop would land on the edge of the growing pillar and would break due to the impact speed of the drop, spaying part of its volume towards the base of the pillar while leaving most of it at the top.

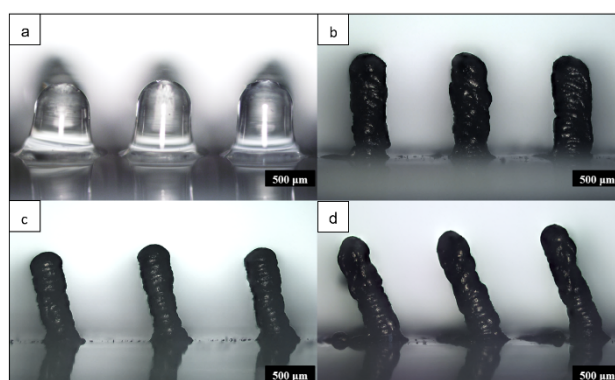


Figure 9. Self-standing pillars perpendicular to the substrate printed with photo-curable resin (a) and carbon paint (b). Small shifts in the pattern after each layer lead to pillars with 12° (c) and 21° (d) of inclination.

Soluble supports

Once both the conductive and structural materials were characterised, several proof-of-concept samples were created to show the capabilities of the high viscosity approach. First, the solubility in water of the carbon paste was used to explore the possibility of printing more complex structures using a soluble

support material, which is an approach that other Additive Manufacturing techniques are already implementing in order to be able to create overhangs and hollow structures. Therefore, the sample shown in Figure 10 was created alternating the use of each material during the print. Specifically, the structure was divided in different “structural blocks” containing a different number of layers of each material in order to compensate their miss-match in thickness, as is described in Table 3. Also, due to the bigger diameter of the photoactive resin and their more noticeable spreading after deposition than that observed for the carbon paste, all the required layers of support material were printed first in each “structural block”, providing a guiding space for the structural material. This method worked reasonably well but it is the main factor of the curved profiles of the hollow channels observed in Figure 10, since they are in fact the profile of the support material before being dissolved.

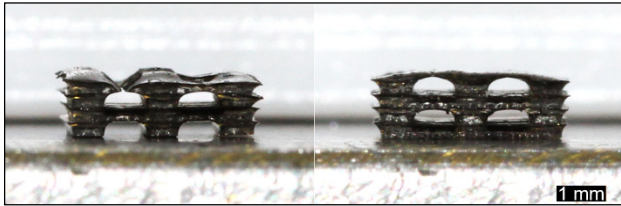




Figure 10. Two lateral views of a woodpile structure printed with the aid of the carbon paste as a water-soluble support material.

Table 3. Description of structural blocks and materials used for the creation of a woodpile structure (Figure 10)

Patterns	Material (function)	Number of layers
	Carbon (support)	5
	Photo-polymer (structural)	7

Furthermore, the “structural blocks” approach was also used to create the spiral sample shown in Figure 11 with the printing steps given in Table 4. There it can be seen again how this method is providing good results in terms of overhangs that would be impossible without the presence of a support material. However, the miss-match of these two particular materials does not seem to be perfectly compensated, since the superior layers still display some curvature. Also, in the central column the same backbone-like effect that was observed on Figure 10 is present. Again, this is the consequence of the curvature of the support material, which cannot be removed completely but it can probably be reduced by printing thinner “structural blocks”, which will be further investigated in the future work.

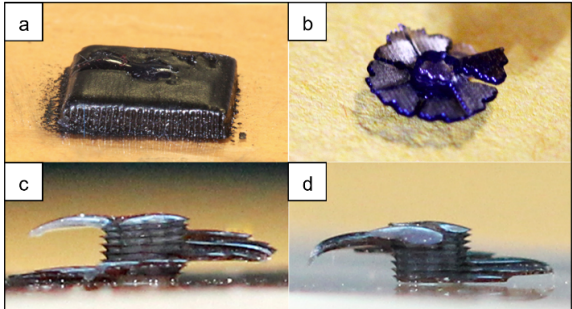




Figure 11. Spiral structure embedded on a cuboid of support material before dissolution (a). The cuboid has dimensions of 7,8 x 7,8 x 1,5 mm. General view of the spiral structure after the support was dissolved in water (b). Lateral views of the spiral structure (c and d).

Table 4. Description of structural blocks and materials used for the creation of a spiral structure (Figure 11)

Patterns	Material (function)	Number of layers
	Carbon (support)	4
	Photo-polymer (structural)	6

Embedded electronics

Additionally, the carbon paste was tested as a conductive material to create embedded tracks, which was the original reason to choose this particular formulation. Therefore, the same approach based on “structural blocks” was applied to create the sample presented in Figure 12 with the structural blocks described in Table 5. The presented device has three embedded tracks, the one in the middle runs flat across the length of the structure until it is raised at the other end, leaving its top surface exposed to act as a capacitive sensing electrode. The other two tracks start flat but then are raised to form a bridge over the middle electrode, providing current to the LED. Finally, the three electrodes are connected with jumper wires to different pins on a micro-controller, which will be in charge of controlling the capacitive sensor and light the LED when presence is detected. Additionally, the whole device is encapsulated on the photo-curable resin to extend its lifetime, however an external frame of carbon is printed to control the spreading of the resin and increase the sharpness of the design. This external frame was later removed with water, taking advantage of the solubility of the material. Once the component was finished it was tested with the 5V supplied by the micro-controller, showing the desired behaviour. This indicates that the printed tracks were not interrupted or shorted at any point and that their resistance was not a hindrance for the emission of light by the LED.

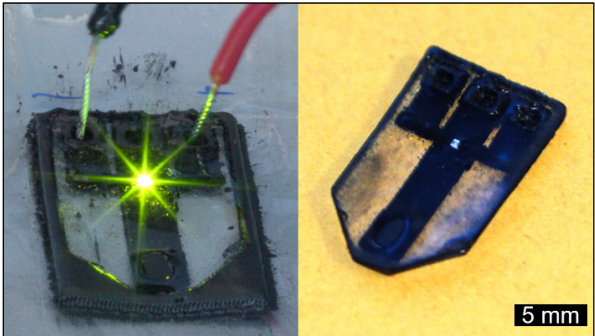




Figure 12. Functional demonstrator containing conductive tracks of carbon paint and a commercial embedded LED. The middle track is independent of the other two and acts as a capacitive switch. The sample was tested with 5V (left). The outer frame of carbon was dissolved with water to achieve a higher resolution (right).

Table 5. Description of structural blocks and materials used for the creation of a functional demonstrator (Figure 12)

Patterns	Material (function)	Number of layers
	Carbon (support and conductive)	4
	Photo-polymer (structural)	5

Conclusions

A high viscosity drop-on-demand approach to the fabrication of multi-material 3-dimensional structures was explored. To do it, a water soluble carbon paint and a photo-curable resin were chosen as functional materials and their viscosity tested with the combination of a rotary and a microfluidic rheometer. The former was particularly useful to determine behaviour closer to storage or rest conditions while the latter provided the viscosity at a shear rate more comparable to the actual shear rates applied to the sample during ejection. From this characterisation and following experiments can be concluded that both Newtonian and non-Newtonian fluids can be jetted with these micro-dispensing valves. However, the higher viscosity at all tested shear rates together with the apparent yield stress of the carbon paint prevented its excessive spreading on the substrate, leading to higher resolution. Therefore, it seems reasonable to conclude that Bingham plastics have the desirable characteristics to be used with this kind of set-up and will be explored further in the future.

Additionally, a method involving the automatic analysis of droplets generated with different configurations was also presented. This provided similar conclusions that the ones previously obtained analysing high speed videos of the ejection in such configurations but in a shorter time [11]. This method, if implemented completely on the system instead of using an external microscope, can significantly speed up the optimization process for new materials. Once the drop formation and deposition were fixed, the resolution and post-treatment were studied. In particular, the carbon paint required between 30 and 300 seconds to completely dry at room temperature. Allowing the evaporation of the solvent during 5 minutes resulted in a linear growth of the sample with successive layers. This was satisfactory for the study here presented but thermal treatments should be studied in the future to obtain the same results in a fraction of the time. Similarly, the photo-polymer was cured with a UV-lamp at 6 and 150 mm/s, observing that the fastest method not only was more suitable in terms of process speed but also pinned the fluid faster to the substrate, partially limiting the negative effects of material spreading. These post-treatments were put to use in the successful fabrication of self-standing pillars. The photo-resin flow properties did not allow the creation of tilted pillars, but the carbon showed promising results up to 21°. Finally, the conductivity and water solubility of the carbon paint and the transparency and structural integrity of the photo-polymer were combined to produce 3-dimensional structures. Particularly remarkable is the final demonstrator that combines all these properties into a functional device capable of switching on and off an embedded LED responding to a capacitive switch. This proves that the studied method is capable of producing such complex structures and open many opportunities in the area of multi-material and multi-functional fabrication.

Finally, it is noteworthy that the materials tested in this work were originally formulated for other applications, such as brush painting and stereolithography, but were used successfully without any modification. This brings the encouraging conclusion that many more materials nowadays on the market intended for technologies such as screen-printing, robocasting, extrusion or moulding could be incorporated effortlessly to the jetting catalogue.

References

- [1] D. Y. Shin, Y. Lee, and C. H. Kim, "Performance characterization of screen printed radio frequency identification antennas with silver nanopaste", *Thin Solid Films*, 517, 21, pp. 6112–6118 (2009).
- [2] D. Deganello, J. A. Cherry, D. T. Gethin, and T. C. Claypole, "Patterning of micro-scale conductive networks using reel-to-reel flexographic printing", *Thin Solid Films*, 518, 21, pp. 6113–6116 (2010).
- [3] T. Sekitani, Y. Noguchi, U. Zschieschang, H. Klauk, and T. Someya, "Organic transistors manufactured using inkjet technology with subfemtoliter accuracy", *Proc. Natl. Acad. Sci.*, pp. 4976–80 (2008).
- [4] P. Calvert, D. Duggal, P. Patra, A. Agrawal, and A. Sawhney, "Conducting Polymer and Conducting Composite Strain Sensors on Textiles", *Mol. Cryst. Liq. Cryst.*, 484, 1, p. 291–302 (2008).
- [5] V. Subramanian, J. M. J. Frechet, P. C. Chang, D. C. Huang, J. B. Lee, S. E. Molesa, A. R. Murphy, D. R. Redinger, and S. K. Volkman, "Progress Toward Development of All-Printed RFID Tags: Materials, Processes, and Devices", *Proc. IEEE*, 93, 7, pp. 1330–1338, (2005).
- [6] S. Magdassi, Ed., *The chemistry of inkjet inks*. (World Scientific, 2010).
- [7] M. Hedges and A. Marin, "3D Aerosol Jet Printing-Adding Electronics Functionality to RP/RM", *DDMC 2012 Conference*, pp. 1–5 (2012).
- [8] S. a. Elrod, B. Hadimioglu, B. T. Khuri-Yakub, E. G. Rawson, E. Richley, C. F. Quate, N. N. Mansour, and T. S. Lundgren, "Nozzleless droplet formation with focused acoustic beams", *J. Appl. Phys.*, 65, 9, p. 3441 (1989).
- [9] D. W. Rosen, L. Margolin, and S. Vohra, "Printing High Viscosity Fluids Using Ultrasonic Droplet Generation", *International Solid Freeform Fabrication Symposium – An Additive Manufacturing Conference*, pp. 239–253 (2008).
- [10] H. Yang, Y. He, C. Tuck, R. Wildman, and R. Hague, "High viscosity jetting system for 3D reactive inkjet printing", *International Solid Freeform Fabrication Symposium – An Additive Manufacturing Conference*, pp. 505–513 (2013).
- [11] J. Ledesma-Fernandez, C. Tuck, and R. Hague, "High Viscosity Jetting of Conductive and Dielectric Pastes for Printed Electronics", *International Solid Freeform Fabrication Symposium – An Additive Manufacturing Conference*, pp. 40–55, (2015).
- [12] Nordson EFD, *PICO x MOD Valve Operating Manual*, (Nordson EFD, 2013).
- [13] C. J. Pipe, T. S. Majmudar, and G. H. McKinley, "High shear rate viscometry", *Rheol. Acta*, 47, 5–6, pp. 621–642, (2008).
- [14] Malvern Instruments Limited, "Quantifying shear thinning behavior on a rotational rheometer using the power law model" (2014).
- [15] J. Duffy, "Optimizing high-performance ceramic inkjet inks", *Paint & Coatings Industry*, September, pp. 1–4, (2014).
- [16] H. Barnes, *A handbook of elementary rheology*. (University of Wales, Institute of Non-Newtonian Fluid Mechanics, 2000).

Author Biography

Javier Ledesma-Fernandez received his BSc in physics at the University of Valencia in 2011. In 2012 he obtained the "La Caixa Foundation" scholarship and continued his studies with a MSc in the area of nanoscience at the Bristol Centre for Functional Nanomaterials. Later he joined the Additive Manufacturing and 3D Printing Research Group at Nottingham University where he is currently completing his PhD thesis on the jettability of high viscosity materials for multifunctional Additive Manufacturing